GluK2 Q/R editing regulates kainate receptor signalling and synaptic AMPA receptor expression and function.

Jithin D. Nair[1], Kevin A. Wilkinson[1], Christophe Mulle[3], Bryce Vissel[4],

Jack Mellor[2]* and Jeremy M. Henley[1]*

[1] Centre for Synaptic Plasticity, School of Biochemistry, Centre for Synaptic Plasticity, Biomedical Sciences Building, University of Bristol, University Walk, Bristol, BS8 1TD, UK.

[2] Centre for Synaptic Plasticity, School of Physiology, Pharmacology and Neuroscience, Biomedical Sciences Building, University of Bristol, University Walk, Bristol, BS8 1TD, UK.

[3] CNRS UMR 5297, Interdisciplinary Institute of Neuroscience, University of Bordeaux, France.

[4] Centre for Neuroscience and Regenerative Medicine, St Vincent's Hospital, Sydney, Australia.

Abstract

Q/R editing of kainate receptor (KAR) subunit GluK2 pre-mRNA replaces a genetically encoded glutamine to an arginine residue in the channel pore to alter the biophysical and trafficking properties of assembled KARs in recombinant systems. However, the consequences of GluK2 Q/R editing *in vivo* remain largely unexplored. Here we investigated differences between GluK2-editing deficient mice, that express ~95% unedited GluK2(Q) compared to wild-type counterparts that express ~85% edited GluK2(R). At hippocampal mossy fibre-CA3 (MF-CA3) synapses the editing-deficient (GluK2(Q)) mice displayed enhanced postsynaptic KAR function and increased KAR-mediated presynaptic facilitation, demonstrating heightened ionotropic function. Conversely, KAR-mediated metabotropic function, measured by regulation of afterhyperpolarization currents, was reduced in GluK2(Q) mice. Moreover, GluK2(Q) mice had fewer GluA1-containing synaptic AMPA receptors (AMPARs) and reduced postsynaptic AMPAR currents at MF-CA3 synapses. Using patterns of stimulation that replicate physiological activity, we show that GluK2(Q) mice have reduced long-term potentiation of AMPAR-mediated transmission at Schaffer collateral synapses. These findings indicate that GluK2 Q/R editing influences the balance of ionotropic versus metabotropic KAR signalling and regulates synaptic AMPAR expression and plasticity.

Kainate receptors (KARs) are glutamate-gated cation channels That are assembled from tetrameric combinations of the subunits GluK1-GluK5. Depending on the synapse and neuron type, KARs are present at both pre- and post-synaptic sites throughout the brain. Despite their close homology to AMPA and NMDA type of glutamate receptors, postsynaptic KARs mediate only a minor fraction of the ionotropic synaptic response to glutamate but are critically important for synaptic integration and regulation of neural circuits (1-3). Presynaptic KARs also contribute to neuronal network function by regulating neurotransmitter release probability at both excitatory and inhibitory synapses (4-10).

Pre- and postsynaptic KARs have been particularly well studied at hippocampal glutamatergic MF-CA3 synapses (11, 12) where the GluK2 subunit is an integral component of both pre- and post-synaptic KARs (5-7, 13-15). Ionotropic postsynaptic KARs containing GluK2 were first discovered at MF-CA3 synapses (11, 12, 16) and presynaptic GluK2 containing KARs contribute to short-term plasticity of presynaptic release probability over timescales ranging from 10ms to 20s (17, 18).

In addition to ionotropic actions, KARs also initiate G-protein coupled metabotropic signalling (19-23). Pharmacological activation of KARs by exogenous agonists regulates presynaptic release of both GABA and glutamate through a metabotropic action (19, 24). Under physiological conditions, metabotropic signalling through KARs has been demonstrated at Schaffer collateral CA1 synapses (25) and at Mf-CA3 synapses (14, 26). In these studies, synaptic activation of postsynaptic KARs inhibits slow after hyperpolarization (I_{sAHP}), a long-lasting voltage independent and Ca^{2+}-dependent K^+ current produced following short bursts of action potentials (27). KAR-mediated inhibition of I_{sAHP} occurs in multiple neuronal types via a $G_{i/o}$ G protein and PKC-dependent pathway and, in CA3 cells, is absent in GluK2 knockout mice, suggesting a crucial role for this subunit in this form of metabotropic signalling (14, 25, 26, 28).

KAR surface expression is activity-dependent and bidirectionally regulated (23, 29-33). Furthermore, activation of KARs can also up- or down regulate AMPAR surface expression and plasticity (23, 34). For example, in cultured hippocampal neurons transient, selective activation of GluK2-containing KARs increases AMPAR surface expression and at Schaffer collateral-CA1 synapses in hippocampal slices GluK2-containing KARs can induce AMPAR long-term potentiation (KAR-LTP_{AMPAR}) via a pertussis toxin-sensitive metabotropic signalling pathway (23). In contrast, sustained activation of KARs in cultured hippocampal neurons reduces surface expression of AMPARs and induces AMPAR long-term depression (KAR-LTD_{AMPAR}) in CA1 neurons in hippocampal slices, an effect that is lost in the absence of GluK2

(34). These results highlight the importance of GluK2-containing KARs as modulators of AMPAR-mediated synaptic transmission.

GluK2 pre-mRNA can be Q/R edited by the enzyme ADAR2, which replaces a genetically encoded glutamine (Q) residue in the channel pore region to arginine (R) (35, 36). In recombinant systems KARs containing GluK2(R) subunits display ER retention and reduced traffic to the surface compared to those assembled with the unedited GluK2(Q) (37, 38) and surface expressed edited GluK2(R)-containing receptors do not gate Ca^{2+} and have a conductance of <1% of GluK2(Q) (39). Furthermore, GluK2 Q/R editing is dynamically regulated to mediate homeostatic plasticity of KARs (32). Specifically, chronic suppression of network activity decreases ADAR2 levels, reducing editing of GluK2 and leading to enhanced KAR surface expression. Reciprocally, chronic enhancement of network activity promotes GluK2 Q/R editing and reduces surface expression of the receptor (31-33).

In this study we investigated how GluK2 Q/R editing alters KAR signalling and function in intact neuronal circuits and whether these changes, in turn, regulate AMPAR function. To test the physiological role of GluK2 Q/R editing we used GluK2 editing-deficient (GluK2(Q)) mice. These mice contain a deletion in the intronic editing complementary sequence (ECS) of the *grik2* gene that directs ADAR2-mediated codon substitution in GluK2 pre-mRNA (Figure 1A). This results in >95% of GluK2-KARs in adult mice containing unedited GluK2(Q) whereas KARs in WT mice contain <15% GluK2(Q) (40). GluK2(Q) mice are viable and surface expressed KARs in cultures from these mice display the inwardly rectifying current/voltage relationship, consistent with unedited GluK2-containing KARs expressed in recombinant systems (41, 42). A previous study has demonstrated that GluK2(Q) mice exhibit no differences from WT in the expression levels of GluK2 mRNA, editing of other RNA editing sites in GluK2 (I/V and Y/C), or in Q/R editing of AMPAR GluA2 subunits (40). The GluK2(Q) mice do, however, have increased susceptibility to kainate-induced seizures and display a form of NMDAR-independent LTP at the medial perforant-DG synapses that is not present in WT mice (40).

We used acute hippocampal slices from WT and GluK2-editing deficient mice that express almost exclusively un-edited GluK2(Q). Our data demonstrate that there is enhanced pre- and postsynaptic KAR ionotropic function in the GluK2(Q) mice compared to WT controls. In addition, there is reduced metabotropic KAR-mediated inhibition of I_{sAHP} in the GluK2(Q) mice. We further show that loss of GluK2 editing reduces AMPAR-mediated transmission at MF-CA3 synapses, decreases synaptic levels of GluA1 and attenuates LTP at CA1 Schaffer collateral synapses. We interpret these data to reveal that GluK2 editing is important for determining the mode of KAR signalling which in turn has downstream effects on the expression of synaptic AMPARs.

Results

Enhanced postsynaptic KAR currents at MF-CA3 synapses in GluK2(Q) mice.

Un-edited GluK2(Q) have a higher conductance than edited GluK2(R) containing KARs measured in recombinant systems (39, 43) and disrupting ADAR2-mediated GluK2 Q/R editing enhances the surface expression, single channel conductance, and Ca^{2+} permeability of postsynaptic KARs in cultured neurons (32, 39, 44). Therefore, we first tested whether the editing of GluK2-containing KARs affects basal postsynaptic KAR function by comparing KAR-mediated synaptic responses at MF-CA3 synapses between WT and GluK2(Q) mice. Because the glutamate receptor complement at MF-CA3 synapses and presynaptic facilitation are mature and stable after the 2nd postnatal week (45, 46) we used P14-P21 mice. We confirmed stability of AMPAR and KAR expression across this age range in the 3rd postnatal week

To compare between GluK2-editing deficient and WT genotypes, we used a minimal stimulation approach to isolate the synaptic response evoked by stimulation of a single presynaptic mossy fibre axon at 3Hz in acutely prepared hippocampal slices (45). Postsynaptic responses were recorded from CA3 pyramidal neurons in whole-cell voltage clamp configuration in the presence of picrotoxin (50μM) and D-APV (50μM) to block $GABA_A$Rs and NMDARs, respectively. The stimulation intensity applied to presynaptic axons increased incrementally until a postsynaptic response was observed (Figure 1B). Interestingly, the percentage of trials that evoked a synaptic response (success rate) was decreased in the GluK2(Q) mice (Figure 1C) (WT=43 ± 5%, GluK2(Q)=27 ± 1%; unpaired t-test, p=0.017) suggesting either a reduced number of release sites or reduced probability of glutamate release from the same number of sites. The AMPAR antagonist GYKI53655 (40μM) was then applied to pharmacologically isolate KAR-mediated excitatory postsynaptic currents ($EPSC_{KA}$) evoked by single presynaptic mossy fibre axons. Analysis of detectable synaptic responses revealed that $EPSC_{KA}$ increased in amplitude in GluK2(Q) mice (Figure 1D) (WT=4.66 ± 0.63pA, GluK2(Q)=7.31 ± 0.50pA; unpaired t-test, p=0.0057) but with no change in decay kinetics (Figure 1E) (τ_{decay}, WT=16.0 ± 1.5ms, GluK2(Q)=13.9 ± 1.1ms; unpaired t-test, p=0.28), consistent with enhanced conductance of un-edited GluK2(Q)-containing receptors (39, 43).

To further test this change in $EPSC_{KA}$ amplitude we also measured the $EPSC_{KA}$ – to $EPSC_{AMPA}$ amplitude ratio for both minimal and larger EPSCs evoked by bursts of 3 stimuli at 167Hz given to mossy fiber axons that recruited multiple axons. $EPSC_{AMPA}$s were first collected in the presence of picrotoxin (50μM) and D-APV (50μM) to block $GABA_A$Rs and NMDARs, respectively. Then, $EPSC_{KA}$s were isolated by blocking $EPSC_{AMPA}$ with bath application of GYKI53655 (40μM) for 10 mins. The $EPSC_{KA}/EPSC_{AMPA}$ ratio increased in GluK2(Q) mice

(Figure 1F, G) (Minimal stimulation: WT=0.049 ± 0.005, GluK2(Q)=0.12 ± 0.007; unpaired t-test, p= 0.0001; 167Hz stimulation: WT=0.047 ± 0.005, GluK2(Q)= 0.086 ± 0.008; unpaired t-test, p=0.0008). This increase in KAR/AMPAR ratio could result from an increase in $EPSC_{KA}$, or a decrease in $EPSC_{AMPA}$, or both. However, in combination with the minimal stimulation $EPSC_{KA}$ data, the increase in KAR/AMPAR ratio supports the contention that $EPSC_{KA}$s are increased in GluK2(Q) mice.

Enhanced presynaptic facilitation in GluK2(Q) mice

Presynaptic KARs at MF-CA3 synapses act as autoreceptors activated by the release of glutamate to facilitate the probability of vesicle release in response to subsequent action potentials (7, 47-49). Therefore, to determine how GluK2 editing affects presynaptic KAR function at MF-CA3 synapses, we examined short-term facilitation of presynaptic release in the presence of picrotoxin (50μM) across the range of timescales.

By measuring $EPSC_{AMPA}$, we examined paired-pulse facilitation (PPF) at 50ms stimulation interval and accumulation of frequency facilitation (FF) at 1s stimulation interval in acute slices from WT and GluK2(Q) mice. Both PPF and FF were increased in GluK2(Q) mice (Figure 2A, B) (PPF: WT=3.3 ± 0.2, GluK2(Q)=5.3 ± 0.6; un-paired t-test, p=0.0067; FF: WT=4.5 ± 0.4, GluK2(Q)=6.6 ± 0.6; unpaired t-test, p=0.0114), indicating enhanced presynaptic KAR function and/or decreased basal release probability. In all our experiments the purity of mossy fiber input was determined by addition of the group II metabotropic glutamate receptor agonist DCG-IV (2μM) (50) with recordings excluded if there was <70% inhibition of synaptic responses. Furthermore, to exclude the possibility that differences in the purity of mossy fibre inputs contributed to the enhanced short-term facilitation in GluK2(Q) mice we analysed the degree of DCG-IV inhibition. No differences were observed (Figure 2C) (WT=91.5 ± 2.1%, GluK2(Q)=93.2 ± 1.2%; unpaired t-test, p=0.4879) and there was no correlation between degree of inhibition by DCG-IV and PPR (Supplementary Figure-S1A, B) (WT, r=0.277, R^2=0.0769, p=0.383; GluK2(Q), r=-0.280, R^2=0.0784, p=0.378; 95% confidence interval). Furthermore, there was no correlation between EPSC amplitude and PPR (Supplementary Figure-S1 C,D) (WT, r=0.127, R^2=0.0163, p=0.692; GluK2(Q), r=0.0383, R^2 = 0.00147, p=0.906; 95% confidence interval) and EPSC initial amplitudes in response to the first stimulus were set to be similar between genotypes (WT=156.6 ± 14.4pA, GluK2(Q)=143.9 ± 17.8pA; unpaired t-test, p=0.5830) and.

Taken together with the reduced success rate observed in the minimal stimulation experiments (Figure 1C), these data indicate that basal release probability at MF-CA3 synapses is reduced in GluK2(Q) mice and that presynaptic facilitation is enhanced..

Impaired metabotropic KAR function in GluK2(Q) mice

KARs signal via ionotropic and metabotropic mechanisms. Q/R editing is predicted to affect ionotropic signalling since the Q/R site is within the conducting pore but the effects on metabotropic signalling are unknown. Therefore, to assess the effects of Q/R editing on metabotropic function we measured KAR inhibition of the slow afterhyperpolarization current (I_{sAHP}) in acute hippocampal slices (14, 25, 26, 51). I_{sAHP} currents were evoked in whole-cell voltage clamped CA3 pyramidal cells by depolarising the membrane potential to 0mV from -50mV for 200ms in the presence of 50µM picrotoxin, 50µM D-APV, 40µM GYKI53655 and 1µM CGP55845 to inhibit $GABA_A$Rs, NMDARs, AMPARs and $GABA_B$Rs, respectively (26). Robust and stable I_{sAHP} currents were obtained in both WT and GluK2(Q) mice, with no differences in baseline amplitudes between genotypes (Figure 3A) (WT=67.0 ± 8.0pA, GluK2(Q)=63.1 ± 6.6pA; unpaired t-test, p=0.712). Activation of synaptic KARs by MF stimulation (10 stimuli at 25Hz every 20s for 10mins) (26) produced a consistent depression of I_{sAHP} in WT mice but there was a reduced depression in GluK2(Q) mice (Figure 3B) (WT=45.1 ± 3.7%, GluK2(Q)=26.7 ± 2.7%; unpaired t-test, p=0006). These data show that GluK2(Q) mice have reduced KAR metabotropic signalling.

Altered synaptic KAR subunit expression in GluK2(Q) mice

Impaired KAR metabotropic signalling by Q/R editing deficient mice could arise from disrupted molecular signalling or reduced expression of synaptic KARs. To distinguish between these possibilities, we assessed total KAR expression as well as synaptic KAR expression in synaptosomes prepared from the brains of WT or GluK2(Q) mice. Total expression of the KAR subunits GluK1, GluK2 and GluK5 was unaltered in GluK2(Q) mice (Figure 4A) (GluK1: WT=100 ± 9.1%, GluK2(Q)=105.1 ± 10.5%, unpaired t-test, p=0.72; GluK2: WT=100 ± 13.2%, GluK2(Q)=117.2 ± 19.2 unpaired t-test, p=0.48; GluK5: WT=100.0 ± 7.8%, GluK2(Q)=90.9 ± 10.1%, unpaired t-test, p=0.50). In synaptosomes, however, the expression of GluK1 and GluK2 was reduced whereas expression of GluK5 was increased (Figure 4A) (GluK1: WT=100.1 ± 6.1%, GluK2(Q)=78.8 ± 5.0%, unpaired t-test, p=0.03; GluK2: WT=100 ± 2.9%, GluK2(Q)=76.9 ± 3.9, unpaired t-test, p=0.0041; GluK5: WT=100.0 ± 5.8%, GluK2(Q)=128 ± 8.3%, unpaired t-test, p=0.045). These data indicate that the enhanced pre- and post-synaptic ionotropic KAR function demonstrated in (Figures 1&2) are likely attributable to the increased conductance of GluK2(Q)-containing KARs, rather than an increase in the number of synaptic KARs. Correspondingly, the reduced metabotropic signalling demonstrated in (Figure 3) can be attributed to fewer KARs at synapses to counterbalance the increase in KAR channel conductance.

Since most postsynaptic KARs in the hippocampus comprise heteromeric combinations of GluK2/GluK5 and the auxiliary subunit NETO1 (52), we also examined levels of NETO1 in

synaptosomes and found levels were unchanged (Figure 4B) (WT=100.0 ± 18.8%, GluK2(Q)=98.2 ± 22.6%, unpaired t-test, p=0.95). Interestingly, however, the synaptosomal level of the closely related auxiliary subunit NETO2 was decreased (Figure 4B) (WT=100 ± 17.4%, GluK2(Q)=43.3 ± 12.8%, unpaired t-test, p=0.043).

Reduced synaptic AMPAR expression in GluK2(Q) mice

KARs can regulate the functional surface expression of AMPARs (23, 33). Given that KAR expression and function are altered in GluK2(Q) mice we next tested whether synaptic expression and function of AMPARs was also affected. Intriguingly, synaptosomal levels of the AMPAR subunit GluA1 were reduced (Figure 5A) (WT=100 ± 8.6%, GluK2(Q)=62.0 ± 4.8%, unpaired t-test, p=0.013) whereas levels of GluA2 were unchanged (WT=100 ± 9.12%, GluK2(Q)=88.3 ± 12.9%, unpaired t-test, p=0.49). We also tested NMDARs and found levels of the obligatory NMDAR subunit GluN1 and the preferentially synaptically localised GluN2A (53) were unchanged in GluK2(Q) mice (Figure 5B) (GluN1: WT=100 ± 22.5%, GluK2(Q)=82.4 ± 21.6%, unpaired t-test, p=0.60; GluN2A: WT=100 ± 6.5%, GluK2(Q)=89.2 ± 6.5%, unpaired t-test, p=0.30). These data indicate that GluK2 Q/R editing selectively regulates synaptic levels of both KARs and AMPARs but not NMDARs.

We also tested whether reduced synaptic expression of GluA1 containing AMPARs had functional effects by analysing the minimal stimulation data. The average AMPAR-EPSC amplitude for successful trials was reduced in GluK2(Q) mice (Figure 5C) (WT=94.5 ± 8.8pA, GluK2(Q)=59.1 ± 3.5pA; unpaired t-test, p=0.0044). These data are consistent with a role of GluK2 Q/R editing in maintaining AMPAR-mediated transmission at MF-CA3 synapses. Together, these data demonstrate the role of GluK2 editing in supporting AMPAR expression and function at MF-CA3 synapses.

Impaired LTP at Schaffer collateral-CA1 synapses in GluK2(Q) mice

We next wondered if the reduced synaptic expression of GluA1 containing AMPARs might also have an impact on the expression of long-term potentiation (LTP). Therefore, we tested LTP expression at Schaffer collateral-CA1 synapses, a well characterized NMDAR-dependent form of LTP. Extracellular field potential recordings from acute hippocampal slices revealed that high frequency stimulation that replicates the *in vivo* patterns of hippocampal sharp-wave/ripple-like (RL) activity (23, 54) induced robust LTP of AMPAR-mediated EPSPs in WT mice but LTP was significantly reduced in GluK2(Q) mice (Figure 6A) (WT: 172.8 ± 10.4% in test pathway vs 97.7 ± 3.8% in control pathway; unpaired t-test, p=0.0002; GluK2(Q): 133.8 ± 3.6% in test pathway vs 97.2 ± 4.9% in control pathway; unpaired t-test; p=0.0001; comparison between test pathways, unpaired t-test, p=0.0087). The paired-pulse ratio remained unchanged after induction of LTP in both WT and GluK2(Q) mice (Figure 6B) (WT=2.04 ± 0.14

baseline, 1.74 ± 0.17 after LTP, p=0.325; GluK2(Q)=2.13 ± 0.14 baseline, 1.95 ± 0.11 after LTP, p=0.65; Two-way ANOVA with Sidak's multiple comparison test). These data suggest that KAR Q/R editing reduces basal synaptic AMPAR expression and also impairs the recruitment and trafficking of extrasynaptic AMPARs into the synapse required for LTP.

Discussion

GluK2 Q/R editing is developmentally (36, 55) and activity-dependently regulated (31, 32) to modulate and accommodate distinct synaptic and network diversity. However, how GluK2 editing impacts on KAR function and subsequent downstream AMPAR function has not been explored. To address these outstanding questions we compared WT mice, which contain <15% unedited GluK2(Q), and GluK2 Q/R editing deficient (GluK2(Q)) mice that have >95% unedited GluK2(Q) (40).

KARs containing unedited GluK2(Q) have a much greater single channel conductance than those containing edited GluK2© (150pA compared to <10pA) (39). Therefore, it is predicted that postsynaptic ionotropic KAR function would be enhanced in GluK2(Q) mice. We found this to be the case but the increase we observed (WT=4.66 ± 0.63pA, GluK2(Q)=7.31 ± 0.50pA) was not nearly as great as predicted based on the data from heterologous expression systems. There are several possible reasons why the increase in KAR-EPSC was not so large in GluK2(Q) mice. 1) Our observation that number of expressed GluK1 and GluK2 KAR subunits decrease in synaptosomal preparations suggests that neurons compensate homeostatically for potentially toxic enhanced conductance and high Ca^{2+} permeability by reducing the number of KARs. This in itself is surprising since unedited GluK2(Q)-containing KARs traffic more efficiently to the cell surface (32, 38, 56), but we also note that our synaptosome preparations sampled synapses from across single cerebral hemisphere and do not directly report synaptic receptor surface expression. 2) The percentage of unedited GluK2(Q) is not 100% in the GluK2(Q) mice and the remaining <5% GluK2(R) may have a significant impact on synaptic KAR conductance by preferential incorporation into synaptic KARs. 3) There may also be compensating homeostatic alterations in KAR associated proteins such as NETOs that influence KAR conductance (57-60) although we did not find any changes in the expression of NETO1 in the synaptosomal fraction although there was a reduction in NETO2. 4) It is currently unknown how heteromeric KARs containing GluK2(Q) vs©uK2(R) subunits behave when combined with GluK4/GluK5 in native conditions.

Similarly, the increased conductance and Ca^{2+} permeability of GluK2(Q) containing KARs is predicted to increase presynaptic KAR function resulting in enhanced short-term facilitation at both 50ms (PPF) and 1s (FF) timescales. This is indeed what we found but we also observed

an increase in failure rate in the minimal stimulation experiments. These data suggest an additional factor of reduced basal probability of release, or number of release sites, within the large presynaptic mossy fibre boutons, which on its own is predicted to increase presynaptic facilitation. Minimal stimulation was conducted at a stimulation frequency of 3Hz which is sufficient to engage KAR-mediated FF and therefore is expected to produce a lower failure rate in GluK2(Q) mice. Instead, we observed the opposite suggesting that the reduction in basal probability of release is substantial. Our data cannot distinguish between reduced probability of release and reduced number of release sites and further anatomical investigation will be necessary to address this. Nonetheless, overall, our data indicate that GluK2(Q) mice exhibit enhanced pre- and post-synaptic KAR function.

In stark contrast to their enhanced ionotropic KAR function, GluK2(Q) mice show reduced metabotropic function measured by inhibition of I_{sAHP} at MF-CA3 synapses (14, 25, 26, 51). Possible explanations for the diminished metabotropic KAR signalling in GluK2(Q) mice include the reduction in expression of GluK1 and GluK2 KAR subunits and/or Q/R editing may alter KAR conformational changes that lead to metabotropic signaling. It remains unclear and controversial which, and how, specific KAR subunits contribute to KAR metabotropic signalling. Indeed, it has been proposed by different groups that GluK1, GluK2, or GluK5 are required for G-protein coupling and metabotropic effects (14, 20, 23, 30, 61). Thus, although we cannot draw definitive mechanistic conclusions, our data demonstrate that GluK2(Q) mice show reduced metabotropic KAR signalling and, at the same time, enhanced ionotropic function.

A critical role for metabotropic KAR signaling is regulation of both KAR and AMPAR surface expression. For example, depending on the extent of activation, KARs can enhance or reduce AMPAR surface expression to evoke LTP or LTD via metabotropic signalling (23, 34). Our data also show that GluK2 editing impacts on NMDAR-induced LTP at Schaffer collateral synapses in CA1 with GluK2(Q) mice exhibiting reduced LTP. GluK2(Q) mice also had reduced AMPAR-EPSCs at mossy fibre synapses and less GluA1 in synaptosomal fractions, suggesting that KARs not only regulate activity-dependent GluA1-containing AMPAR trafficking but also maintain basal synaptic levels. These changes were specific to AMPARs, since synaptic levels of the NMDAR subunits GluN1 and GluN2A were unchanged, indicating the loss of AMPARs is not due to wholesale changes in synaptic composition in the editing-deficient mice.

These findings suggest KAR activity mediates the ‘tone’ of synaptic AMPARs at MF-CA3 and Schaffer collateral synapses suggesting a wider role where metabotropic KAR signalling sets the tone of synaptic AMPAR function more broadly. We speculate that this may be a

homeostatic mechanism in which the presence of high-conductance, Ca^{2+}-permeable GluK2(Q)-containing KARs causes a compensatory decrease in Ca^{2+}-permeable GluA1-containing AMPARs to balance synaptic responsiveness. This is similar to the observed effects of KAR signalling on expression of AMPARs during the development of synaptic circuits (46, 62) and suggests that this developmental regulation extends into adulthood.

In adult brain GluK2-containing KARs predominantly comprise edited GluK2(R) with only a sparse subgroup of KARs containing unedited GluK2(Q). Using mice that almost exclusively express only GluK2(Q) we show that the ionotropic/metabotropic balance of KAR signalling is radically altered. Based on these results, we propose that unedited GluK2(Q)-containing KARs primarily or exclusively function as ion channels with enhanced conductance for both mono and/or di-valent cations, whereas the ©ted GluK2(R)-containing KARs act as metabotropic receptors to regulate and maintain network activity.

These findings are important because GluK2Q/R editing is subject to both developmental and activity-dependent control (32). Moreover, the proportion of edited GluK2(R) is increased in patients with a pharmaco-resistant temporal lobe epilepsy (TLE) so the increased conductivity could underpin seizure generation (63). Taken together our data indicate that physiologically and pathologically relevant alterations in GluK2 editing dynamically regulate KAR function, signalling mode and set the threshold for the induction of plasticity. Thus, in conclusion, our results highlight that GluK2Q/R editing acts as a previously unsuspected molecular switch that regulates enigmatic dual-mode capability of KARs to operate via either ionotropic or metabotropic signalling to initiate distinct and diverse downstream pathways.

Materials and methods

Animals

GluK2-editing deficient ECS mice and their WT counterparts (129Sv strain) were created at the Salk Institute by mutated intronic editing complementary sequence (ECS) in *GRIK2* gene that directs ADAR2-mediated codon substitution in GluK2 pre-mRNA. (40).

The mice were housed in groups of 2-4 in standard Individually ventilated (IVC) cages in rooms with temperature maintained between 19-23°C and with 12h light and dark cycles. Cages had sawdust, paper nesting and enriched environment (wooden chews, cardboard tubes etc.). Pups of age P14-P21 were used for the experiments irrespective of sex.

All the animal experiments and procedures were performed in compliance with the UK Animal Scientific Procedures act (1986) and were guided by the Home Office Licensing Team at the

University of Bristol. All animal procedures relating to this study were approved by the Animal Welfare and Ethics Review Board at the University of Bristol (approval number UIN/18/004).

All experiments and analysis were performed blinded to mouse genotype.

Acute hippocampal slice preparation

Cervical dislocation followed by decapitation were performed on P14-21 male and female WT and GluK2(Q) mouse pups. The brain was removed and placed in ice-cold sucrose slicing solution (in mM: Sucrose, 205; KCl, 2.5; $NaHCO_3$, 26; NaH_2PO_4, 1.25; D-Glucose, 10; $CaCl_2$, 0.5; $MgCl_2$, 5) saturated with 95% O_2 and 5% CO_2. Hippocampi were carefully removed and transverse sections of 400µm thickness for Whole-cell recordings and 500 µm for field recordings were obtained using a vibratome (Leica VT 1200s). Slices were kept for recovery in a slice holder containing artificial cerebrospinal fluid (aCSF; in mM: NaCl, 124; KCl, 3; $NaHCO_3$, 24; NaH_2PO_4, 1.25; D-Glucose, 10; $MgSO_4$, 4; $CaCl_2$, 4) for whole-cell recordings and (aCSF; in mM: NaCl, 124; KCl, 3; $NaHCO_3$, 24; NaH_2PO_4, 1.25; D-Glucose, 10; $MgSO_4$, 2; $CaCl_2$, 2) for field recordings saturated with 95% O_2 and 5% CO_2 at 37°C for 20 mins and later transferred to room temperature for at least 30 mins before performing experiments.

Electrophysiology recordings

Whole cell recordings

Hippocampal slices were placed in a submerged holding chamber continuously perfused with oxygenated aCSF at 36.5°C at a flow rate of 3ml per minute. Hippocampal CA3 pyramidal cells were visually identified using DIC optics and patch-clamped in whole-cell configuration using a pulled Harvard borosilicate glass capillary of resistance 5-7M MΩ filled with either caesium based whole-cell solution (in mM: NaCl, 8; $CsMeSO_4$, 130; HEPES, 10; EGTA, 0.5; MgATP, 4; NaGTP, 0.3; QX314.Cl, 5; Spermine, 0.1) or K-Gluconate based (in mM: NaCl, 8; KGluconate, 135; HEPES, 10; EGTA, 0.2; MgATP, 2; NaGTP, 0.3) for I_{sAHP} experiments

The cells were held in voltage clamp mode and evoked EPSCs were obtained by stimulating the mossy fibre pathway with a bipolar stimulating electrode placed in the dentate gyrus hilus layer (or glass monopolar electrode for minimal stimulation experiments). Picrotoxin (50µm) (Sigma:P1675) was included in the aCSF to inhibit $GABA_A$ receptors (except for CA1 field recordings). Cells with series resistance above 30 MΩ or where series resistance changed by >20% were excluded from analysis. To confirm the purity of mossy fibre inputs, the group-II mGluR agonist DCG-IV (2 µM) (Tocris:0975/1) was bath applied for 5-10 mins at the end of experiments with mossy fibre stimulation (26). Recordings were only included in analysis if DCG-IV reduced EPSCs by >70%.

Data were digitized at 10kHz, and low-pass filtered at 2kHz using CED Micro 1401-4 A-D acquisition unit and Axon patch 200B amplifier (Molecular devices). All recordings were obtained using CED Signal 5 software.

CED Signal acquisition software was used to analyze the recorded data. Mean responses were obtained every minute by averaging consecutive traces. EPSC amplitudes were measured from the averaged traces and normalized to the mean EPSC amplitude of baseline.

Minimal stimulation

CA3 pyramidal cells were voltage-clamped at -60mV and MF-EPSCs were evoked by moving a mono-polar stimulating electrode filled with aCSF around the inner border of dentate gyrus granule cells until a response was observed. Stimulation intensity was adjusted just above the threshold for activation of a synaptic response (Figure 2A). Consecutive traces were recorded at a frequency of 3Hz. No prominent polysynaptic activation was observed using this low intensity stimulation. AMPAR-EPSCs were measured for 5-10 mins in the presence of D-APV (50μM) for a minimum of 150 trials. Subsequently, GYKI53655 (40μM) was applied to block AMPAR responses and KAR-EPSCs were measured after 15 mins of GYKI53655 application and for 5-10 mins and a minimum of 150 trials. τ_{decay} for AMPAR and KAR-EPSCs were calculated by single exponential curve fitting feature in CED signal software.

KAR/AMPAR ratio

CA3 pyramidal neurons were voltage clamped at -60mV in the presence of D-APV (50μM) (Hello bio: HB0225) (NMDAR antagonist). Mossy fibres were stimulated with a burst of 3 stimuli at 167Hz every 20s to evoke AMPAR/KAR-EPSCs. Stable AMPAR-EPSCs were recorded for 20 minutes and then KAR-EPSCs were recorded for 20 mins in the presence of the AMPAR antagonist GYKI53655 (40μM) (Hellobio:HB0312). Amplitude of AMPAR-KAR peaks and KAR peaks were measured individually and the ratio of KAR-EPSC to AMPAR-EPSC were calculated.

Paired pulse and frequency facilitation

CA3 neurons in acute hippocampal slices were voltage clamped at -70mV in the presence of Picrotoxin (50μM). To measure PPF, EPSCs were evoked by pairs of stimuli to mossy fibres at an inter-stimulus interval of 50ms, every 20s. Paired pulse ratios were obtained by averaging amplitudes of P1 peak to P2 peak. For FF experiments, single stimuli were given at 0.05Hz for 10 mins before stimulation frequency was increased to 1Hz for 1 min. FF ratios were obtained by averaging the last 20 frames of P1 amplitude at 0.05Hz with the middle 40 frames at 1Hz stimulation. After this stimulation frequency was returned to 0.05Hz. DCG-IV (2μM) was then applied for at least 5 mins to assess purity of MF input.

Slow afterhyperpolarizations (I_{sAHP})

For I_{sAHP} recordings, CA3 pyramidal neurons were voltage clamped at -50mV in the presence of picrotoxin (50μM) ($GABA_AR$ antagonist), D-APV (50μM) (NMDAR antagonist), CGP55845 (1μM) (Hellobio: HB0960) ($GABA_BR$ antagonist) and GYKI53655 (40μM) (AMPAR antagonist). Glass electrodes were filled with whole-cell solution (in mM: NaCl, 8; KGluconate, 135; HEPES, 10; EGTA, 0.2; MgATP, 2; NaGTP, 0.3). I_{sAHP} were induced every 20 s by applying a depolarising voltage step to 0mV for 200 ms and I_{sAHP} amplitude was measured 300ms after returning the membrane potential to -50mV to avoid measurement of medium afterhyperpolarization (I_{mAHP}). Synaptic activation of KARs was induced by bursts of 10 stimuli at 25Hz to the mossy fibres 500ms prior to the induction of I_{sAHP}.

Field potential recordings

Extracellular field potentials (fEPSPs) were recorded from stratum radiatum in CA1 using a 3-5 MΩ glass pipette filled with aCSF. Two stimulation electrodes (bipolar) were positioned on opposite sides of the recording electrodes equidistant from the pyramidal layer to evoke two independent inputs (Stim1 and Stim2). LTP induction protocol was delivered only to Stim1 and was alternately positioned closer to the CA3 region or to subiculum in different recordings. Paired stimuli (50ms inter-stimulus interval) were given every 10 s to each pathway, alternating between the control and test pathway (Stim1 and Stim2). LTP consisted of 20 bursts of 20 stimuli at 200Hz given every 5 s. The recordings were performed in the absence of picrotoxin. fEPSP slopes were measured using CED signal software. The slopes are displayed as a percentage of 10 min baseline. For LTP quantification the values were obtained 21-30 min after LTP induction.

Synaptosomal preparations and Western Blotting

Synaptosomes were prepared from cerebral hemisphere of P14-21 pups using Syn-PER™ Reagent (ThermoFisher Scientific : 87793). After cervical dislocation followed by decapitation of the pups, the brain was removed and cut into two halves (along the cerebral hemispheres). The cerebellum was discarded. Each cerebral hemisphere from the pup was weighed and transferred to a glass homogenizer and the required amount of Syn-PER reagent was added to the tissue (10ml of reagent per gram of tissue). The tissue was homogenized on ice with slow stokes (~10 strokes). The homogenate was transferred to a fresh centrifuge tube and centrifuged at 1200 x g for 10 min at 4°C. The supernatant was transferred to a fresh tube and the pellet was discarded. The supernatant was centrifuged again at 15,000 x g for 20 min at 4°C. The supernatant was discarded, and the pellet was resuspended in 1-2ml of Syn-PER reagent. To the synaptosomal fraction Triton x-100 and SDS were added to a final

concentration of 1% and 0.1%, respectively, and left at 4°C on a rotating wheel for 1hr to lyse synaptosomes and solubilize membrane proteins. The samples were then centrifuged at 16,000 x g for 20 mins to remove insoluble material. Protein quantification was performed on the samples and the final samples for western blotting were prepared by adding 2X sample buffer and boiling at 95°C for 10 mins.

The samples were separated based on molecular weight using Sodium dodecyl sulphate- poly acrylamide gel electrophoresis (SDS PAGE). The gradient composed of 10% acrylamide resolving gel (375mM Tris-HCL pH 8.8, 10% acrylamide, 0.1% SDS, 0.1% APS and 0.01% TEMED) and 5% stacking gel (125mM Tris-HCL pH 6.8, 5% acrylamide, 0.1% SDS, 0.1% APS, 0.01% TEMED) .The gels were transferred to PVDF membrane and blocked in 5% skimmed milk in PBS-T (0.137M NaCl, 2.7mM KCl, 10mM Na_2HPO_4, 2mM K_2HPO_4, pH to 7.4 with HCl) + 0.001% Tween-20) for 1 hr at RT and blotted overnight at 4°C in the same blocking solution with the following antibodies: Rabbit Anti-GluK1 (1:1000; Millipore: 07-258), Rabbit Anti-GluK2/3 (1:1000; Millipore:04-921), Rabbit Anti-GluK5 (1:1000; Millipore:06-315), inhouse Rabbit Anti-Neto1 (1:1000), Rabbit Anti-Neto2 (1:1000; Abcam:Ab109288), Rabbit Anti-GluA1 (1:1000; Millipore:AB1504), Mouse Anti-GluA2 (1:1000, BD Pharmighen:556341), Rabbit Anti-NMDAR1 (1:1000; Abcam:Ab109182), Rabbit Anti NR2A(1:1000), Mouse Anti-β-Actin (1:10000; Sigma:A5441). The HRP-Conjugated secondary antibodies form Merck. Anti-rabbit (raised in goat), and anti-mouse (raised in goat). The antibodies were used in 1:10,000 dilution in 5% milk in PBS-T.

For each experiment, the signal for each condition was divided by the signal from the loading control for that experiment (β-actin). This analysis was performed for each replicate experiment, and for presentation purposes, the mean of the control condition set to 100%.

Data analysis

Data are plotted a– mean ± SEM. 'N' - Number of – animals used, 'n' - number of cells. ANOVA, or paired or unpaired student t-test were used for statistical analysis and stated in the figure legends with respective p values. All statistical tests were performed using GraphPad Prism version 9.3.

Acknowledgements

We are grateful to the BBSRC (BB/R00787X/1), the Leverhulme Trust (RPG-2019-191) and the Wellcome Trust (220799/Z/20/Z) for funding this work.

References

1. M. Frerking, R. A. Nicoll, Synaptic kainate receptors. *Curr Opin Neurobiol* **10**, 342-351. (2000).
2. D. M. Kullmann, Presynaptic kainate receptors in the hippocampus: slowly emerging from obscurity. *Neuron* **32**, 561-564 (2001).
3. J. Lerma, Roles and rules of kainate receptors in synaptic transmission. *Nat Rev Neurosci* **4**, 481-495 (2003).
4. R. Chittajallu *et al.*, Regulation of glutamate release by presynaptic kainate receptors in the hippocampus. *Nature* **379**, 78-81 (1996).
5. A. Contractor, G. Swanson, S. F. Heinemann, Kainate receptors are involved in short- and long-term plasticity at mossy fiber synapses in the hippocampus. *Neuron* **29**, 209-216. (2001).
6. D. Schmitz, J. Mellor, M. Frerking, R. A. Nicoll, Presynaptic kainate receptors at hippocampal mossy fiber synapses. *Proc Natl Acad Sci U S A* **98**, 11003-11008 (2001).
7. S. E. Lauri *et al.*, A critical role of a facilitatory presynaptic kainate receptor in mossy fiber LTP. *Neuron* **32**, 697-709. (2001).
8. H. Kamiya, Kainate receptor-dependent presynaptic modulation and plasticity. *Neurosci Res* **42**, 1-6 (2002).
9. S. Sachidhanandam, C. Blanchet, Y. Jeantet, Y. H. Cho, C. Mulle, Kainate receptors act as conditional amplifiers of spike transmission at hippocampal mossy fiber synapses. *J Neurosci* **29**, 5000-5008 (2009).
10. C. Mulle, V. Crepel, Regulation and dysregulation of neuronal circuits by KARs. *Neuropharmacology* **197**, 108699 (2021).
11. P. E. Castillo, R. C. Malenka, R. A. Nicoll, Kainate receptors mediate a slow postsynaptic current in hippocampal CA3 neurons. *Nature* **388**, 182-188. (1997).
12. M. Vignes, D. Bleakman, D. Lodge, G. L. Collingridge, The synaptic activation of the GluR5 subtype of kainate receptor in area CA3 of the rat hippocampus. *Neuropharmacol.* **36**, 1477-1481. (1997).
13. C. Mulle *et al.*, Altered synaptic physiology and reduced susceptibility to kainate-induced seizures in GluR6-deficient mice. *Nature* **392**, 601-605 (1998).
14. A. Ruiz, S. Sachidhanandam, J. K. Utvik, F. Coussen, C. Mulle, Distinct subunits in heteromeric kainate receptors mediate ionotropic and metabotropic function at hippocampal mossy fiber synapses. *J Neurosci* **25**, 11710-11718 (2005).
15. M. Darstein, R. S. Petralia, G. T. Swanson, R. J. Wenthold, S. F. Heinemann, Distribution of kainate receptor subunits at hippocampal mossy fiber synapses. *J Neurosci* **23**, 8013-8019 (2003).
16. C. Mulle *et al.*, Altered synaptic physiology and reduced susceptibility to kainate-induced seizures in GluR6-deficient mice. *Nature* **392**, 601-605 (1998).
17. P. A. Salin, M. Scanziani, R. C. Malenka, R. A. Nicoll, Distinct short-term plasticity at two excitatory synapses in the hippocampus. *Proc Natl Acad Sci U S A* **93**, 13304-13309 (1996).
18. D. Schmitz, J. Mellor, R. A. Nicoll, Presynaptic kainate receptor mediation of frequency facilitation at hippocampal mossy fiber synapses. *Science* **291**, 1972-1976. (2001).
19. A. Rodriguez-Moreno, J. Lerma, Kainate receptor modulation of GABA release involves a metabotropic function. *Neuron* **20**, 1211-1218. (1998).

20. J. L. Rozas, A. V. Paternain, J. Lerma, Noncanonical signaling by ionotropic kainate receptors. *Neuron* **39**, 543-553 (2003).
21. A. Contractor, C. Mulle, G. T. Swanson, Kainate receptors coming of age: milestones of two decades of research. *Trends Neurosci* **34**, 154-163 (2011).
22. J. Lerma, J. M. Marques, Kainate receptors in health and disease. *Neuron* **80**, 292-311 (2013).
23. M. M. Petrovic *et al.*, Metabotropic action of postsynaptic kainate receptors triggers hippocampal long-term potentiation. *Nat Neurosci* **20**, 529-539 (2017).
24. R. A. Cunha, J. O. Malva, J. A. Ribeiro, Pertussis toxin prevents presynaptic inhibition by kainate receptors of rat hippocampal [(3)H]GABA release. *FEBS Lett* **469**, 159-162 (2000).
25. Z. Melyan, B. Lancaster, H. V. Wheal, Metabotropic regulation of intrinsic excitability by synaptic activation of kainate receptors. *J Neurosci* **24**, 4530-4534 (2004).
26. S. E. Chamberlain, J. H. Sadowski, L. M. Teles-Grilo Ruivo, L. A. Atherton, J. R. Mellor, Long-term depression of synaptic kainate receptors reduces excitability by relieving inhibition of the slow afterhyperpolarization. *J Neurosci* **33**, 9536-9545 (2013).
27. B. Lancaster, P. R. Adams, Calcium-dependent current generating the afterhyperpolarization of hippocampal neurons. *J Neurophysiol* **55**, 1268-1282 (1986).
28. A. Fisahn, S. F. Heinemann, C. J. McBain, The kainate receptor subunit GluR6 mediates metabotropic regulation of the slow and medium AHP currents in mouse hippocampal neurones. *J Physiol* **562**, 199-203 (2005).
29. S. Martin, J. M. Henley, Activity-dependent endocytic sorting of kainate receptors to recycling or degradation pathways. *EMBO J* **23**, 4749-4759 (2004).
30. I. M. Gonzalez-Gonzalez, J. M. Henley, Postsynaptic kainate receptor recycling and surface expression are regulated by metabotropic autoreceptor signalling. *Traffic* **14**, 810-822 (2013).
31. A. J. Evans, S. Gurung, K. A. Wilkinson, D. J. Stephens, J. M. Henley, Assembly, Secretory Pathway Trafficking, and Surface Delivery of Kainate Receptors Is Regulated by Neuronal Activity. *Cell Rep* **19**, 2613-2626 (2017).
32. S. Gurung, A. J. Evans, K. A. Wilkinson, J. M. Henley, ADAR2 mediated Q/R editing of GluK2 regulates homeostatic plasticity of kainate receptors. *bioRxiv* **30865** (2018).
33. J. D. Nair, K. A. Wilkinson, J. M. Henley, J. R. Mellor, Kainate Receptors and Synaptic Plasticity. *Neuropharmacology* 10.1016/j.neuropharm.2021.108540, 108540 (2021).
34. J. D. Nair *et al.*, Sustained postsynaptic kainate receptor activation downregulates AMPA receptor surface expression and induces hippocampal LTD. *iScience* **24**, 103029 (2021).
35. P. H. Seeburg, M. Higuchi, R. Sprengel, RNA editing of brain glutamate receptor channels: mechanism and physiology. *Brain Res Brain Res Rev* **26**, 217-229. (1998).
36. A. Filippini, D. Bonini, L. La Via, A. Barbon, The Good and the Bad of Glutamate Receptor RNA Editing. *Mol Neurobiol* **54**, 6795-6805 (2017).
37. S. Pahl, D. Tapken, S. C. Haering, M. Hollmann, Trafficking of kainate receptors. *Membranes (Basel)* **4**, 565-595 (2014).
38. S. M. Ball, P. T. Atlason, O. O. Shittu-Balogun, E. Molnar, Assembly and intracellular distribution of kainate receptors is determined by RNA editing and subunit composition. *J Neurochem* **114**, 1805-1818 (2010).

39. G. T. Swanson, D. Feldmeyer, M. Kaneda, S. G. Cull-Candy, Effect of RNA editing and subunit co-assembly single-channel properties of recombinant kainate receptors. *J Physiol* **492**, 129-142. (1996).
40. B. Vissel *et al.*, The role of RNA editing of kainate receptors in synaptic plasticity and seizures. *Neuron* **29**, 217-227. (2001).
41. D. Bowie, M. L. Mayer, Inward rectification of both AMPA and kainate subtype glutamate receptors generated by polyamine-mediated ion channel block. *Neuron* **15**, 453-462 (1995).
42. S. K. Kamboj, G. T. Swanson, S. G. Cull-Candy, Intracellular spermine confers rectification on rat calcium-permeable AMPA and kainate receptors. *J Physiol (Lond)* **486**, 297-303 (1995).
43. J. Egebjerg, V. Kukekov, S. F. Heinemann, Intron sequence directs RNA editing of the glutamate receptor subunit GluR2 coding sequence. *Proc Natl Acad Sci USA* **91**, 10270-10274 (1994).
44. W. Paschen, J. Schmitt, C. Gissel, E. Dux, Developmental changes of RNA editing of glutamate receptor subunits GluR5 and GluR6: in vivo versus in vitro. *Brain Res Dev Brain Res* **98**, 271-280 (1997).
45. C. Marchal, C. Mulle, Postnatal maturation of mossy fibre excitatory transmission in mouse CA3 pyramidal cells: a potential role for kainate receptors. *J Physiol* **561**, 27-37 (2004).
46. F. Lanore *et al.*, Deficits in morphofunctional maturation of hippocampal mossy fiber synapses in a mouse model of intellectual disability. *J Neurosci* **32**, 17882-17893 (2012).
47. A. Contractor, G. T. Swanson, A. Sailer, S. O'Gorman, S. F. Heinemann, Identification of the kainate receptor subunits underlying modulation of excitatory synaptic transmission in the CA3 region of the hippocampus. *J Neurosci* **20**, 8269-8278. (2000).
48. A. Rodriguez-Moreno, T. S. Sihra, Presynaptic kainate receptor facilitation of glutamate release involves protein kinase A in the rat hippocampus. *J Physiol* **557**, 733-745 (2004).
49. J. Breustedt, D. Schmitz, Assessing the role of GLUK5 and GLUK6 at hippocampal mossy fiber synapses. *J. Neurosci.* **24**, 10093-10098 (2004).
50. H. Kamiya, S. Ozawa, Dual mechanism for presynaptic modulation by axonal metabotropic glutamate receptor at the mouse mossy fibre-CA3 synapse. *J Physiol* **518 (Pt 2)**, 497-506 (1999).
51. Z. Melyan, H. V. Wheal, Metabotropic actions of kainate receptors in the regulation of I(sAHP) and excitability in CA1 pyramidal cells. *Adv Exp Med Biol* **717**, 49-58 (2011).
52. B. A. Copits, G. T. Swanson, Dancing partners at the synapse: auxiliary subunits that shape kainate receptor function. *Nat Rev Neurosci* **13**, 675-686 (2012).
53. B. van Zundert, A. Yoshii, M. Constantine-Paton, Receptor compartmentalization and trafficking at glutamate synapses: a developmental proposal. *Trends Neurosci* **27**, 428-437 (2004).
54. C. J. Behrens, L. P. van den Boom, L. de Hoz, A. Friedman, U. Heinemann, Induction of sharp wave-ripple complexes in vitro and reorganization of hippocampal networks. *Nat Neurosci* **8**, 1560-1567 (2005).

55. A. Bernard *et al.*, Q/R editing of the rat GluR5 and GluR6 kainate receptors in vivo and in vitro: evidence for independent developmental, pathological and cellular regulation. *Eur. J. Neurosci.* **11**, 604-616. (1999).
56. A. J. Evans, S. Gurung, J. M. Henley, Y. Nakamura, K. A. Wilkinson, Exciting Times: New Advances Towards Understanding the Regulation and Roles of Kainate Receptors. *Neurochem Res* 10.1007/s11064-017-2450-2 (2017).
57. M. S. Wyeth *et al.*, Neto auxiliary protein interactions regulate kainate and NMDA receptor subunit localization at mossy fiber-CA3 pyramidal cell synapses. *J Neurosci* **34**, 622-628 (2014).
58. Y. J. Li *et al.*, Neto proteins regulate gating of the kainate-type glutamate receptor GluK2 through two binding sites. *J Biol Chem* **294**, 17889-17902 (2019).
59. C. Straub *et al.*, Distinct functions of kainate receptors in the brain are determined by the auxiliary subunit Neto1. *Nat Neurosci* **14**, 866-873 (2011).
60. C. Straub, W. Zhang, J. R. Howe, Neto2 modulation of kainate receptors with different subunit compositions. *J Neurosci* **31**, 8078-8082 (2011).
61. I. Rutkowska-Wlodarczyk *et al.*, A Proteomic Analysis Reveals the Interaction of GluK1 Ionotropic Kainate Receptor Subunits with Go Proteins. *J Neurosci* **35**, 5171-5179 (2015).
62. S. E. Lauri *et al.*, Synaptic activation of a presynaptic kainate receptor facilitates AMPA receptor-mediated synaptic transmission at hippocampal mossy fibre synapses. *Neuropharmacology* **41**, 907-915. (2001).
63. G. Kortenbruck, E. Berger, E. J. Speckmann, U. Musshoff, RNA editing at the Q/R site for the glutamate receptor subunits GLUR2, GLUR5, and GLUR6 in hippocampus and temporal cortex from epileptic patients. *Neurobiol Dis* **8**, 459-468 (2001).

Figure 1: Enhanced postsynaptic KAR currents at MF-CA3 synapses in GluK2(Q) mice

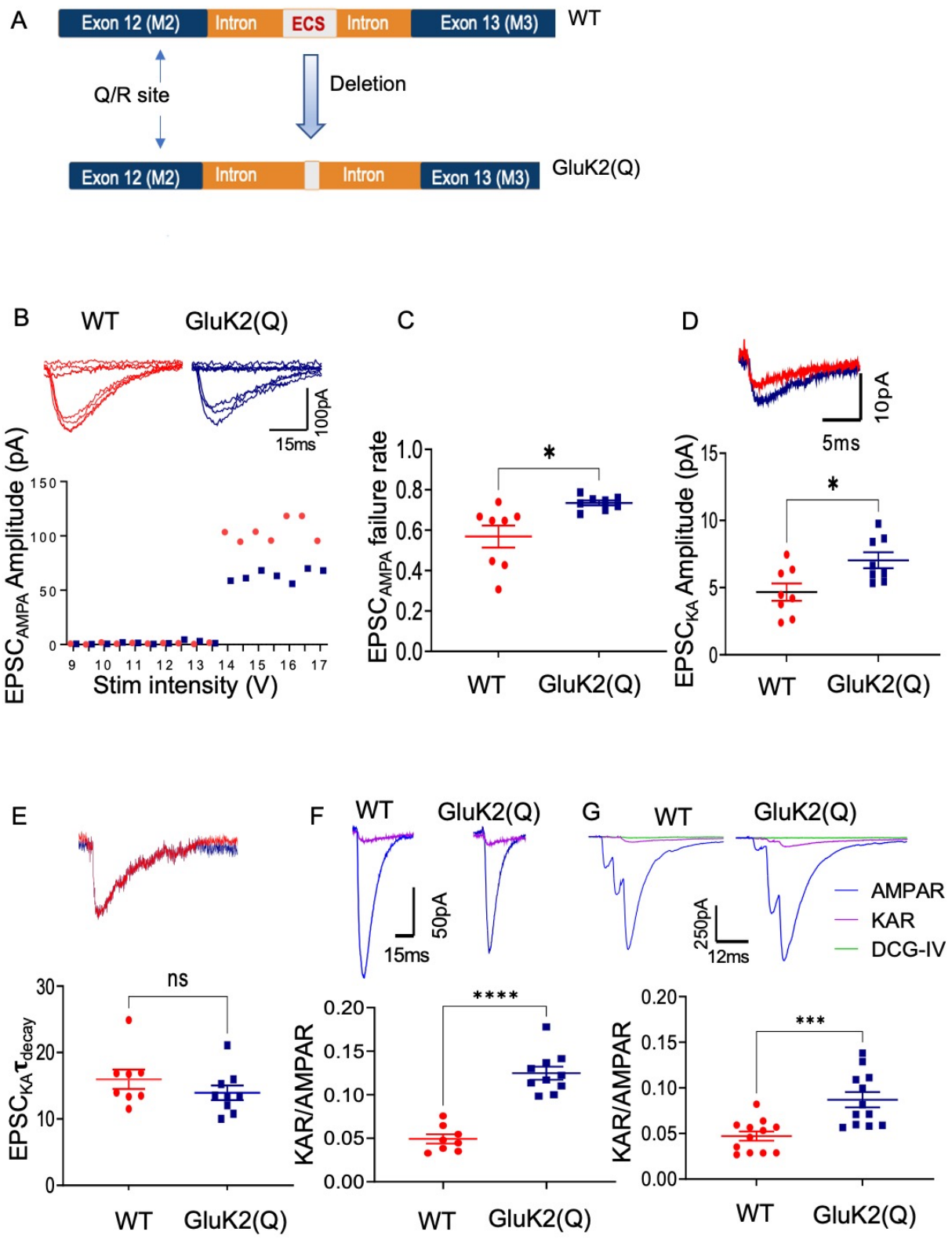

Figure 1: Enhanced postsynaptic KAR currents at MF-CA3 synapses in GluK2(Q) mice

(A) The intronic region between exon 12 (M2) and 13 (M3) in the *Grik2* gene contains an editing complementary site (ECS), located ~1900nt downstream of exon 12. In the WT mice, this region is intact. However, in homozygous GluK2(Q) mice, a 600bp region is deleted from the ECS site. This prevents ADAR2 binding and subsequent editing of GluK2 pre-mRNA at Q/R site, leading to the translation of 95% un-edited GluK2(Q) subunits.

(B) Superimposed 8 consecutive traces showing success and synaptic failures for minimal stimulation for WT (top left) and GluK2(Q) mice (top right)**.** Representative data from a minimal stimulation experiment showing stimulation intensity threshold for evoking responses from excitation of a single axon fibre (bottom).

(C) Quantification of probability of failures for AMPAR responses out of 150 stimulations in WT and GluK2(Q) mice N=5, n=8 cells for WT and N=5, n=10 cells for GluK2(Q) mice (bottom); ns $p>0.05$, *$p<0.05$, **$p<0.01$; unpaired t-test with Welch's correction.

(D) Representative trace showing $EPSC_{KA}$ in WT and GluK2(Q) mice (top). Quantification of average amplitude of $EPSC_{KA}$ (bottom). N=5, n=8 cells for WT and N=5, n=10 cells for GluK2(Q) mice (bottom); ns $p>0.05$, *$p<0.05$, **$p<0.01$; unpaired t-test with Welch's correction.

(E) Representative trace showing τ_{decay} for KAR currents (scaled) in WT vs GluK2(Q) (top) Quantification of τ_{decay} for KAR currents in WT vs GluK2(Q) mice. N=5, n=8 cells for WT and N=5, n=10 cells for GluK2(Q) mice (bottom); ns $p>0.05$, *$p<0.05$, **$p<0.01$; unpaired t-test with Welch's correction.

(F) Representative traces showing postsynaptic AMPAR and KAR currents in WT and GluK2(Q)mice with minimal stimulation (top). Quantification of KAR/AMPAR current ratio in WT and GluK2(Q)mice (bottom) for WT and N=5, n=10 cells for GluK2(Q) mice, ns $p>0.05$, ****$p<0.0001$; unpaired t-test with Welch's correction.

(G) Representative traces showing postsynaptic AMPAR and KAR currents in WT and GluK2(Q)mice with burst stimulation at 167Hz (top). Quantification of KAR/AMPAR current ratio in WT and GluK2(Q)mice(bottom). N=5, n=12 cells, ns $p>0.05$, *$p<0.05$, **$p<0.01$; unpaired t-test with Welch's correction.

Figure 2: Enhanced presynaptic facilitation in GluK2(Q) mice

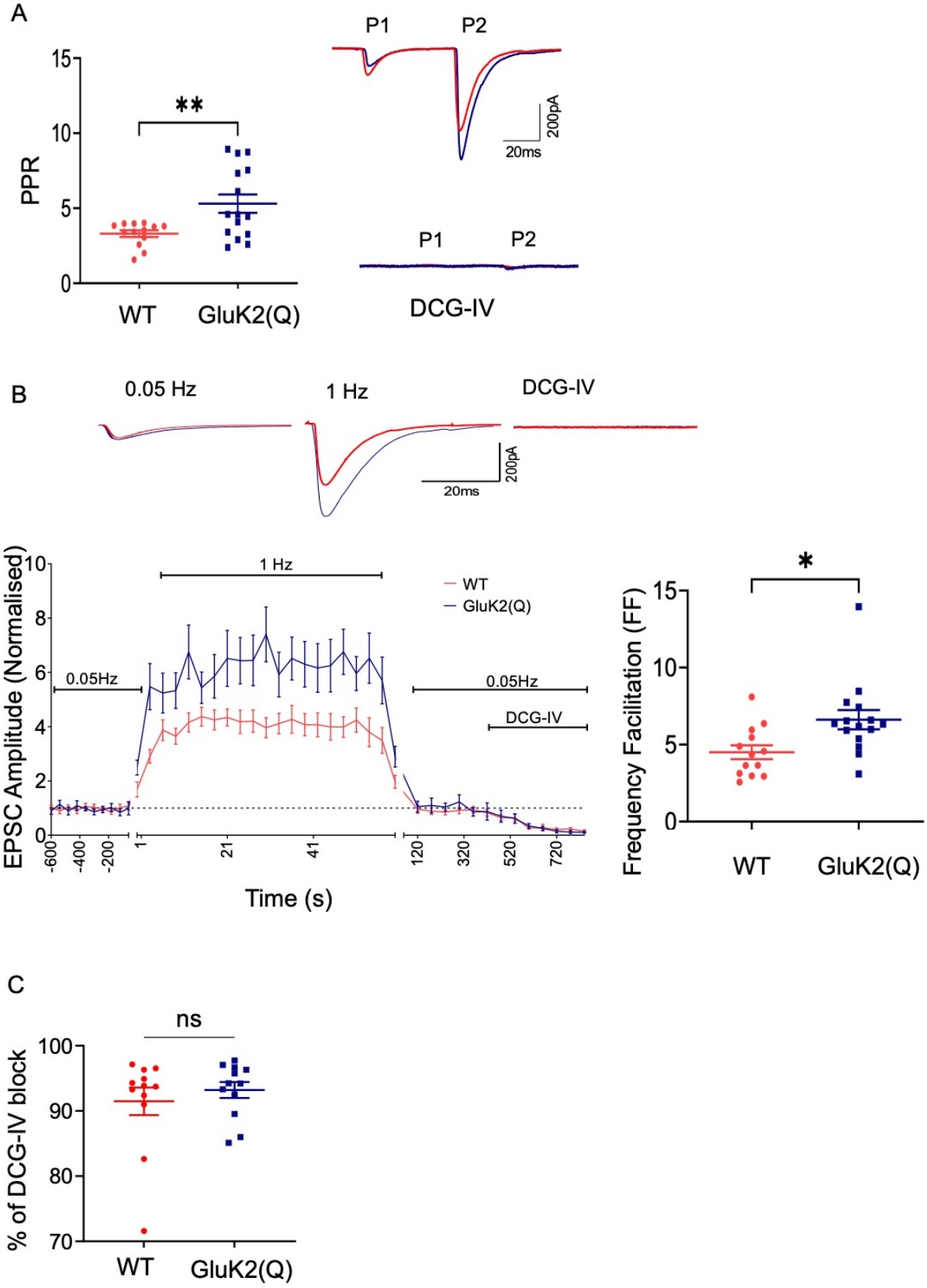

Figure 2: Enhanced presynaptic facilitation in GluK2(Q) mice

(A) Quantification of average paired-pulse ratio in WT and GluK2(Q) mice (left). Representative traces showing EPSCs in response to paired pulse stimulation from both WT and GluK2(Q) mice before (top right) and after DCG-IV application (bottom right). WT, N=7, n=13 cells; GluK2(Q) mice, N=8, n=15 cells; ns $p>0.05$, *$p<0.05$, **$p<0.01$; unpaired t-test with Welch's correction.

(B) Representative trace showing frequency facilitation from WT and GluK2(Q) mice (top). Timeline of frequency facilitation experiments in WT and GluK2(Q) mice (bottom left). Quantification of frequency facilitation in WT and GluK2(Q) mice (bottom right).

(C) Percentage of DCG-IV block in WT and GluK2(Q) mice . WT, N=7, n=13 cells; GluK2(Q) mice, N=8, n=15 cells; ns $p>0.05$, *$p<0.05$, **$p<0.01$; unpaired t-test with Welch's correction.

Figure 3: Impaired metabotropic KAR function in GluK2(Q) mice

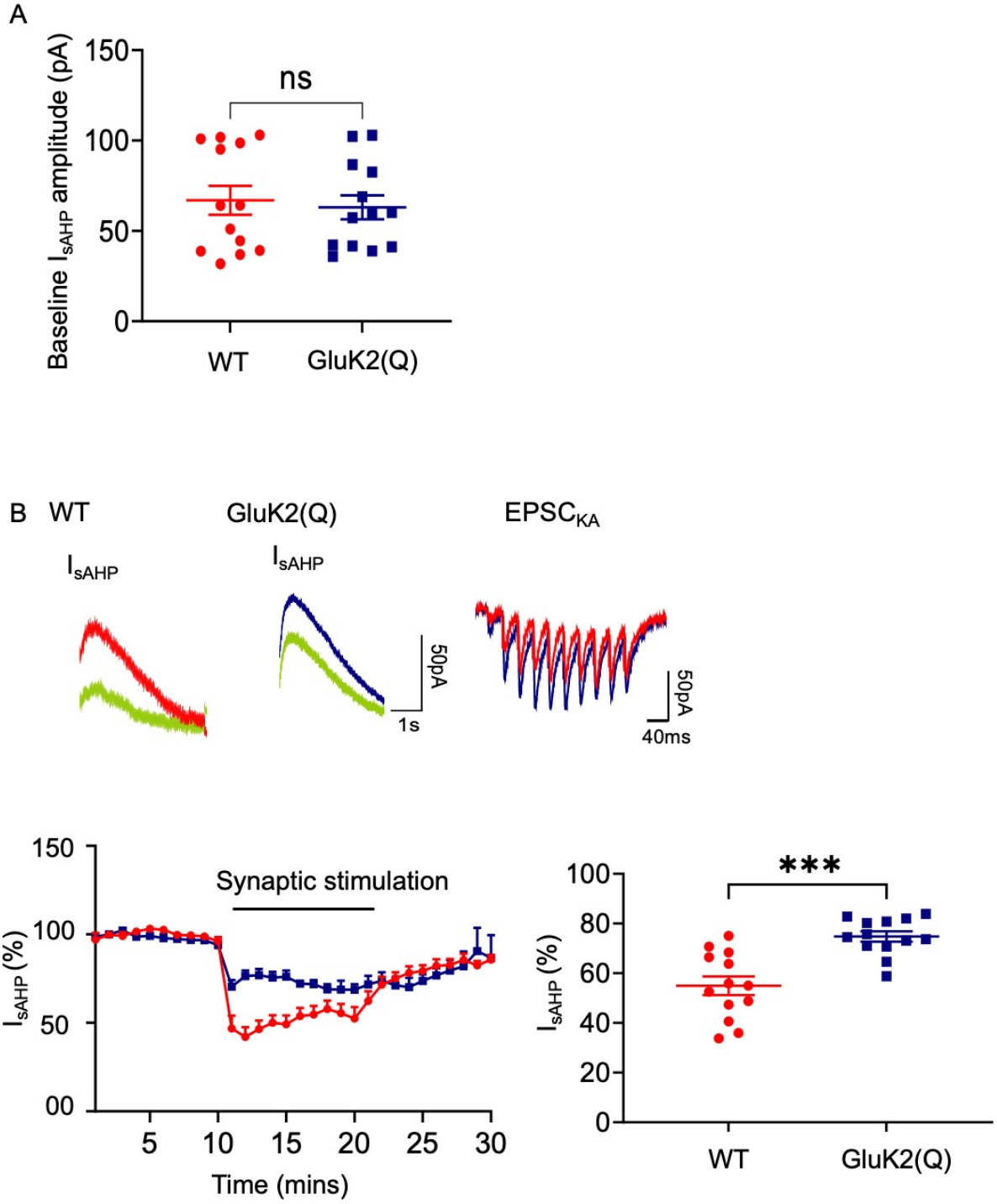

Figure 3: Impaired metabotropic KAR function in GluK2(Q) mice

(A) Average baseline amplitude of I_{sAHP} currents in WT and GluK2(Q) mice.
(B) Sample traces from WT (top left), GluK2(Q) mice (top middle) and $EPSC_{KA}$ following synaptic stimulation (top right). Timeline showing inhibition of I_{sAHP} following synaptic KAR activation (bottom left). Quantification of percentage inhibition of I_{sAHP} following synaptic KAR activation in WT and GluK2(Q) mice (bottom right). N=4 animals, n=13 cells, ns $p>0.05$, **$p<0.0001$; un-paired t test with Welch's correction.

Figure 4: Altered synaptic KAR subunit expression in GluK2(Q) mice

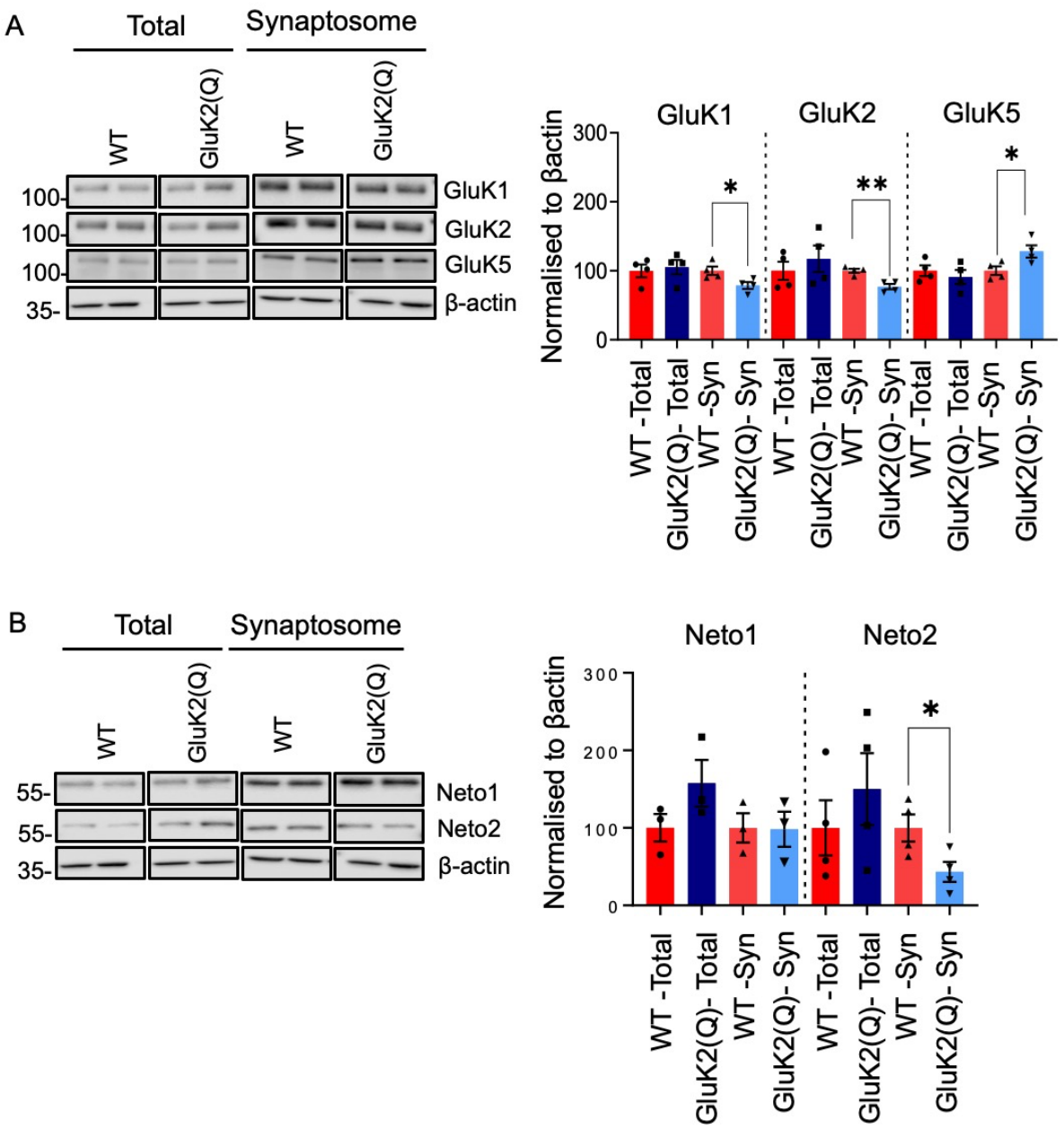

Figure 4: Altered synaptic KAR subunit expression in GluK2(Q) mice

(A) Representative western blots of total and synaptosomal fraction samples from single cerebral hemisphere of WT and GluK2(Q) mice for KAR subunits (left) . Quantification of proteins expressed as percentage of WT protein after normalizing to β actin (right). β actin was used as a loading control. N=4 animals; ns $p>0.05$, *$p<0.05$, **$p<0.01$; unpaired t-test with Welch's correction.

(B) Representative western blots of total and synaptosomal fraction samples from single cerebral hemisphere of WT and GluK2(Q) mice for auxiliary KAR subunits NETO1 and NETO2 (left) Quantification of proteins expressed as percentage of WT protein after normalizing to β actin (right). β actin was used as a loading control N=3 animals; ns $p>0.05$, *$p<0.05$, **$p<0.01$; unpaired t-test with Welch's correction.

Figure 5: Reduced synaptic AMPAR expression in GluK2(Q) mice

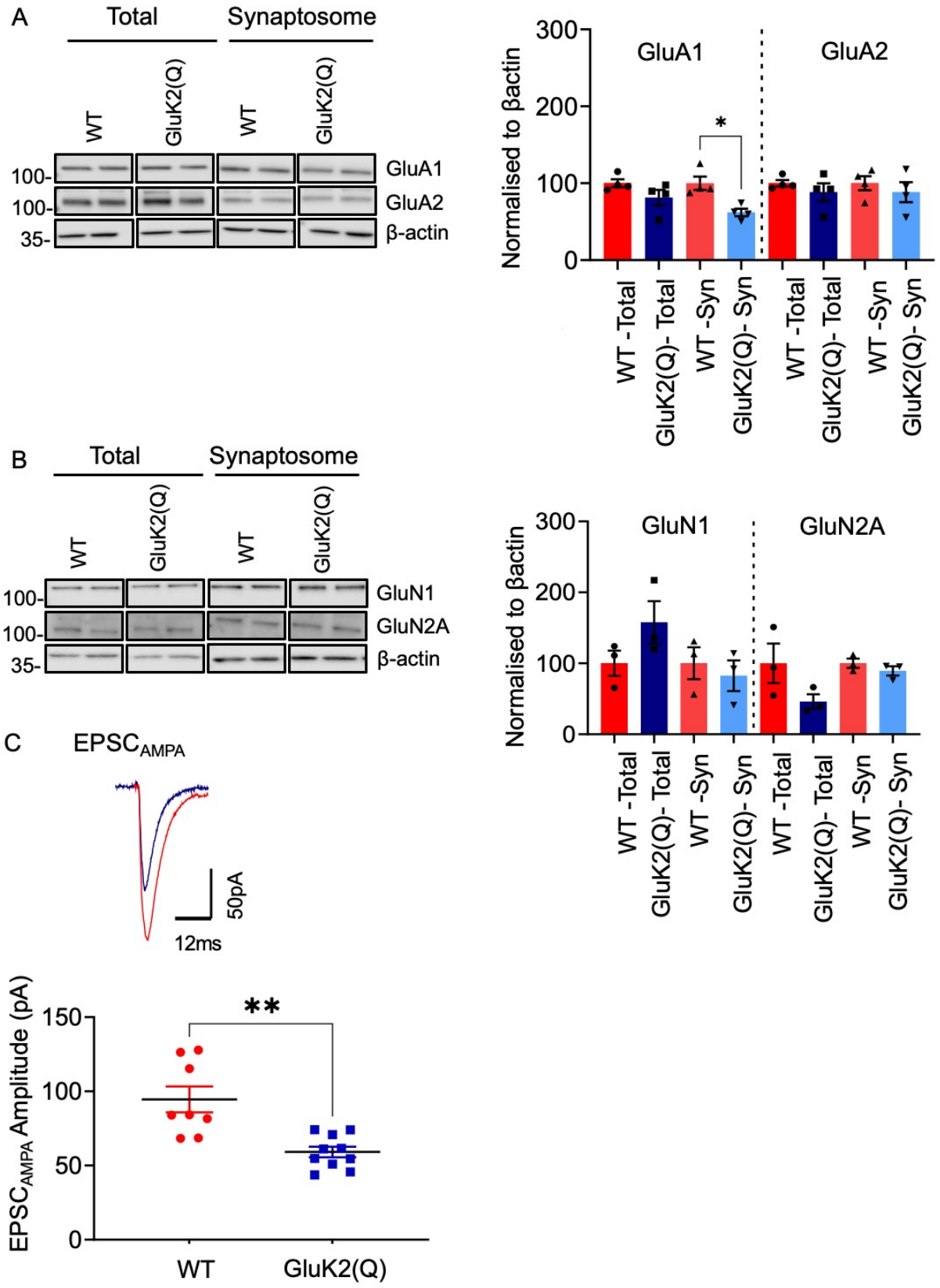

Figure 5: **Reduced synaptic AMPAR expression in GluK2(Q) mice**

(A) Representative western blots of total and synaptosomal fraction samples from single cerebral hemisphere of WT and GluK2(Q) mice for AMPAR subunits GluA1 and GluA2 (left) . Quantification of proteins expressed as percentage of WT protein after normalizing to β actin (right). β actin was used as a loading control. N=4 animals; ns $p>0.05$, *$p<0.05$, **$p<0.01$; unpaired t-test with Welch's correction.

(B) Representative western blots of total and synaptosomal fraction samples from single cerebral hemisphere of WT and GluK2(Q) mice for NMDAR subunits GluN1 and GluN2A (left). Quantification of proteins expressed as percentage of WT protein after normalizing to β actin (right). β actin was used as a loading control N=3 animals (B); ns $p>0.05$, *$p<0.05$, **$p<0.01$; unpaired t-test with Welch's correction.

(C) Representative trace showing $EPSC_{AMPA}$ in WT and GluK2(Q) mice (top). Quantification of average amplitude of $EPSC_{AMPAR.}$ (bottom) N=5, n=8 cells; ns $p>0.05$, *$p<0.05$, **$p<0.01$; unpaired t-test with Welch's correction.

Figure 6: Impaired LTP at Schaffer collateral-CA1 synapses in GluK2(Q) mice

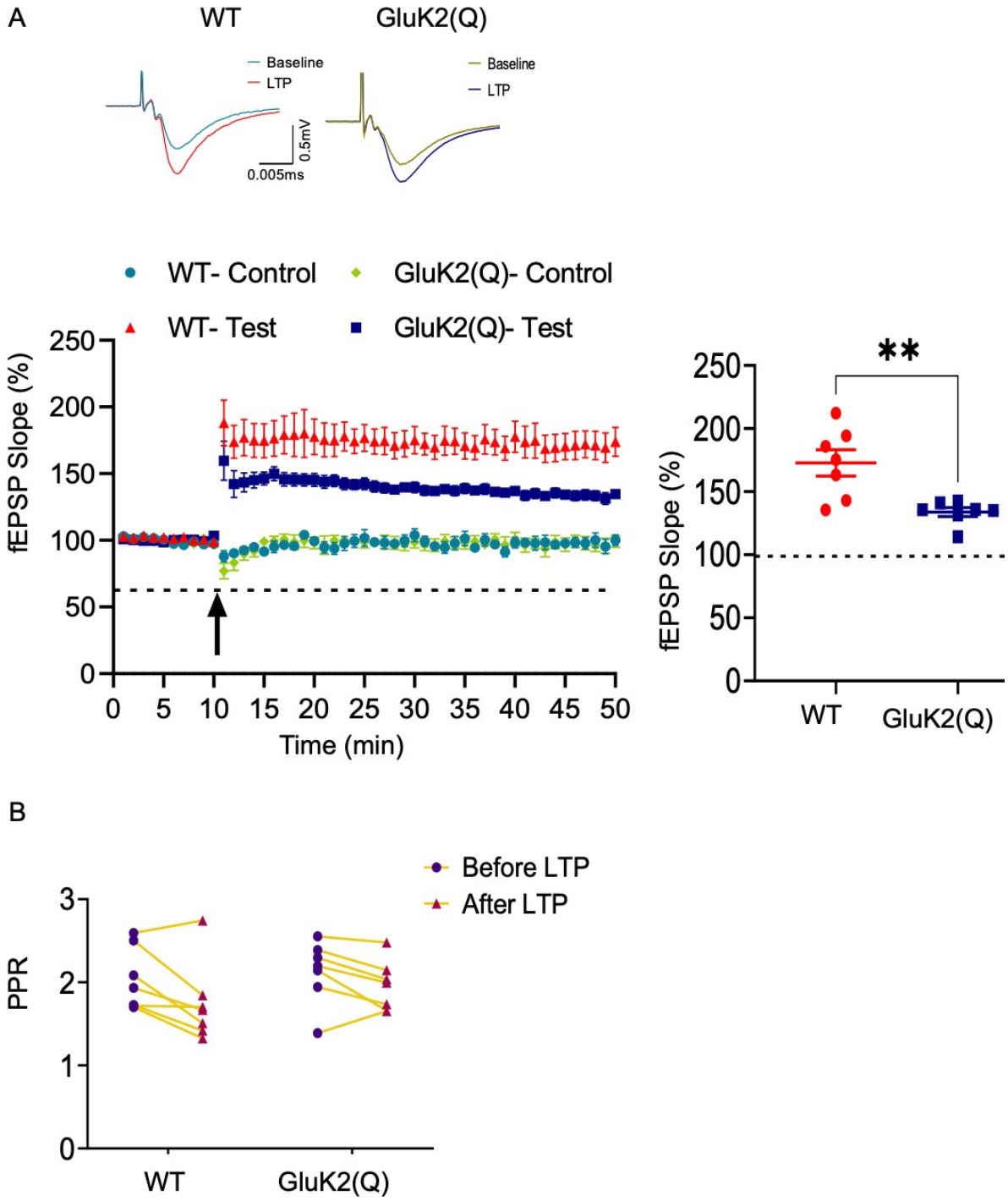

Figure 6: Impaired LTP at Schaffer collateral-CA1 synapses in GluK2(Q) mice

(A) Representative traces showing field EPSP (fEPSP) before and after LTP induction (21-30 min) in WT (top left) and GluK2(Q) mice (top right). Timeline showing fEPSP slope expressed as percentage of baseline subjected to Ripple Like (RL)-LTP induction (Arrow) (bottom left). Normalised fEPSP slope in test pathway 21-30 min after LTP induction in WT and GluK2(Q) mice (bottom right).

(B) Paired-pulse ratio in WT and GluK2(Q) mice before and after LTP induction. N=4 animals, n=7 cells; ns $p>0.05$, **$p<0.002$, ***$p<0.0002$, ****$p<0.0001$; Un-paired t test with Welch's correction; Two-way ANOVA with Sidak's multiple comparison test for PPR.